On Antenna Impedances in a Cold Plasma with a Perpendicular Static Magnetic Field

JANIS GALEJS

Abstract—**A flat strip antenna is embedded in a magnetoionic medium with its longitudinal axis perpendicular to the static magnetic field. The antenna characteristics differ for antennas oriented with their surfaces parallel and perpendicular to the static magnetic field. In the former case there are no resistance peaks for frequencies near the plasma frequency and the reactance of a short antenna is capacitive for low frequencies. For frequencies near the gyrofrequency the antennas are electrically longer for the parallel orientation of their surfaces. The accuracy of the solutions is illustrated by computing the tangential electric surface fields that are excited by the approximate current distributions used in the impedance computations.**

I. Introduction

THE ANTENNA impedances in a cold plasma have been recently calculated by the author [1], [2], for parallel and perpendicular directions of the static magnetic field. These two papers, which contain detailed references of past work will be referred to throughout. In these papers, the antenna impedance was computed using a variational technique which also yielded estimates of the current distribution on the antenna. Several approximate current distributions resulted in nearly the same impedance figures, but there have been no criteria for estimating the accuracy of the current distributions. For the parallel direction of the static magnetic field [1] the impedance data was shown to agree closely with results of earlier investigations, but there have been several discrepancies for antennas with their longitudinal axis perpendicular to the static magnetic field. For frequencies below the plasma frequency the antenna resistance differs from calculations of Seshadri [3], who considered a strip antenna in a uniaxial medium with the static magnetic field perpendicular to the antenna axis, but parallel to the antenna surface. Balmain [4] has deduced a capacitive antenna reactance for a cylindrical current element, while [2] showed an inductive reactance for a flat strip antenna.

This paper considers a flat strip antenna in the x-z plane with the static magnetic field applied in the z-direction which is perpendicular to the antenna axis and parallel to its surface. The antenna is of length $2l$ and width 2ϵ and is excited at its center. The antenna impedance is computed variationally and approximate current distributions are determined from the stationary character of this impedance.

For a transmitting antenna, the tangential electric fields produced by the antenna current should be equal to zero on a perfectly conducting antenna surface, but they differ from zero only in the exciting antenna gap. Such boundary conditions are the basis for formulating the integral equation for the antenna current, which may be solved either by iteration [5] or by numerical methods [6]. This paper examines the degree to which approximate current distributions satisfy this boundary condition by calculating the integrated electric field

$$\int_{-x_1}^{x_1} E_x(x)dx$$

where $x_1<l$. The tangential electric fields $E_x(x)$ should vanish on the perfectly conducting antenna surface, and the above integral should remain constant for an accurately determined current distribution if x_1 corresponds to a point on the metallic antenna surface. Fluctuations of this integral are indicative of inaccuracies in the current distributions [7].

A crude estimate of the antenna impedance can be obtained using an assumed current distribution in the induced EMF method that is based on the conservation of the complex power. Such calculations provide results identical to variational calculations for a similarly assumed current distribution [8], but there are no means for ascertaining a priori the adequacy of a given assumption. It is preferable to start with a more accurate solution and to examine antenna geometries where simpler assumptions can be justified.

Closed-form expressions for the antenna impedance are derived only in the low-frequency limit for short antennas in a uniaxial medium. Most of the results on antenna impedances and all of the results on current distributions are made available in numerical form only.

II. Field Expressions in the Plasma Medium

Assuming a suppressed exp $(-i\omega t)$ harmonic time dependence of the fields for a source free medium, the electric and magnetic vectors E and H satisfy the Maxwell's equations with the dyadic permittivity defined as in (1) to (6) of [1]. The field components F_{ij} in the anisotropic medium are related to their Fourier transforms $\overline{F}_{ij}$ by the integrals

$$F_{ij}(x, y, z) = \left(\frac{1}{2\pi}\right)^2 \int_{-\infty}^{\infty}\int_{-\infty}^{\infty} \overline{F}_{ij}(u, w)e^{iux+iwz}e^{iv_jy}du\,dw, \tag{1}$$

where $F=E$ or H, $i=x, y$, or z, and where subscript j denotes a mode characterized by a particular value of v_j. The relations between v_j and the transform variables u and w will be

Manuscript received May 29, 1968. This work was supported in part by Contract AF19(628)-5718 with the Air Force Cambridge Research Laboratories, USAF Office of Aerospace Research.

The author is with the Applied Research Laboratory, Sylvania Electric Products, Inc., Waltham, Mass. 02154

determined in the subsequent development. Substituting (1) into (1) and (2) of [1], the field components $\overline{E}_x$ and $\overline{H}_x$ can be expressed in terms of $\overline{E}_z$ and $\overline{H}_z$ as

$$\overline{E}_{xj} = \frac{1}{\rho_j^2}\left[- u\frac{k_{zj}^2}{w}\overline{E}_{zj} - \omega\mu_0 v_j \overline{H}_{zj}\right] \tag{2}$$

$$\overline{H}_{xj} = \frac{1}{\rho_j^2}\left[v_j\omega\epsilon_0\epsilon_3\overline{E}_{zj} - uw\overline{H}_{zj}\right], \tag{3}$$

where $\rho_j^2 = u^2 + v_j^2$, $k_{zj}^2 = k_0^2\epsilon_3 - \rho_j^2$, and $k_0 = \omega\sqrt{\mu_0\epsilon_0}$. Equations (2) and (3) are identical to (2) and (4) of [2] if iw is substituted for γ. The same substitution is applied to (6) of [2], and it follows that v_j is determined from the solution of

$$\begin{aligned} 2v_j^2 = {} & \left(p^2 + q^2 - \frac{\epsilon_2^2}{\epsilon_1}k_0^2\right) \pm \left\{(p^2 - q^2)^2 \right. \\ & + \frac{\epsilon_2^2}{\epsilon_1}k_0^2\left[\frac{\epsilon_2^2}{\epsilon_1}k_0^2 - 2k_0^2(\epsilon_1 - \epsilon_3)\right. \\ & \left.\left. + 2w^2\left(1 + \frac{\epsilon_3}{\epsilon_1}\right)\right]\right\}^{1/2} \end{aligned} \tag{4}$$

where

$$p^2 = \epsilon_3 k_0^2 - u^2 - \frac{\epsilon_3}{\epsilon_1}w^2 \tag{5}$$

$$q^2 = \epsilon_1 k_0^2 - u^2 - w^2. \tag{6}$$

Equation (4) can be recognized as the Booker quartic, and its two solutions represent the ordinary and the extraordinary modes. For $w \to 0$, (4) represents a cylindrical wave which propagates radially, i.e., transverse to the applied magnetic field with no variation in the z-direction. Its wave number has the values ρ given by (9) of [2], where the subscripts correspond to the + or − signs of (4). Following a convention used by Arbel and Felsen [9], a solution of (4), which gives for transverse propagation ($w = 0$) a wave number $\rho = \sqrt{\epsilon_3}k_0$, is designated as the ordinary mode. The plus sign in the solution (4) represents, therefore, the ordinary mode (subscript $j = +$), while the minus sign gives the extraordinary mode ($j = -$).

In the presence of a strong static magnetic field $\epsilon_2 \to 0$, and the anisotropic medium becomes uniaxial with $\epsilon_3 \neq \epsilon_1$. The two solutions of (4) become

$$\begin{aligned} v_+^2 &= p^2 \\ v_-^2 &= q^2 \end{aligned} \tag{7}$$

where p and q are defined by (5) and (6).

Equation (4) characterizes only v^2 and there is still an ambiguity of sign in the definition of v. For complex values of v^2 the imaginary part of v should be larger than zero in order to obtain exponentially attenuated fields (1) for large values of y. In this paper, the plasma is considered slightly lossy and the sign of v_j is uniquely determined from the requirement Im $v_j > 0$ for $y > 0$.

The amount of coupling between the TE and TM modes in the anisotropic medium is determined by the admittance

$$Y_j = \frac{\overline{H}_{zj}}{\overline{E}_{zj}}. \tag{8}$$

It follows from (13) of [2] that

$$Y_j = \left[\epsilon_3(k_0^2\epsilon_1 - w^2) - \epsilon_1\rho_j^2\right]/(i\omega\mu_0 w\epsilon_2). \tag{9}$$

Substituting (7) in (9) and letting $\epsilon_2 \to 0$, it follows that $Y_\mp \sim \epsilon_2^2/\epsilon_2 \to 0$ and $\overline{H}_{z+} = 0$ due to an excitation by $\overline{E}_{z\mp}$. Similarly it follows that $|Y_-| \to \infty$ and $\overline{E}_{z-} = 0$ due to an excitation by $\overline{H}_{z-}$.

The above calculation was carried out for $y > 0$. For $y < 0$ the signs of v_j are reversed in (1), (2), and (3). The mode amplitudes $\overline{E}_{zj}$ may differ for $y > 0$ and $y < 0$, and they will be denoted as $\overline{E}_{jp}$ and $\overline{E}_{jn}$, respectively. Noting that $\overline{H}_{zj}$ is related to $\overline{E}_{zj}$ by (8), the four unknown mode amplitudes $\overline{E}_{+p}$, $\overline{E}_{-p}$, $\overline{E}_{+n}$, and $\overline{E}_{-n}$ are determined from the following four boundary conditions for $y = 0$: $\overline{E}_x$, $\overline{E}_z$, and $\overline{H}_x$ are continuous, and $\overline{H}_{zp} = \overline{H}_{zn} + \overline{J}$, where

$$\overline{J} = \int_{-\infty}^{\infty}\int_{-\infty}^{\infty} J_x e^{-iux}e^{-iwz}dx\,dz \tag{10}$$

is the transform of the linear source current density J_x. A lengthy calculation shows that

$$\begin{aligned} \left.\begin{matrix}\overline{E}_{+p} \\ \overline{E}_{+n}\end{matrix}\right\} = {} & \frac{\overline{J}/2}{Y_+ - Y_-}\left\{\pm 1 + \frac{u\epsilon_2}{i\epsilon_1 v_+\rho_-^2}\right. \\ & \left.\left[k_0^2\epsilon_3 - \frac{iw}{\omega\epsilon_0\epsilon_2}Y_-(\epsilon_1 k_0^2 - w^2)\right]\right\}. \end{aligned} \tag{11}$$

The plus and minus signs of the right-hand side refer to subscripts p and n, respectively. The expressions for $\overline{E}_{-p}$ and $\overline{E}_{-n}$ are obtained by interchanging the subscripts + and − in (11). The axial electric field $\overline{E}_x$ at $y = 0$ can be related by (2) and (11) to the transform of the current density $\overline{J}$ as

$$\begin{aligned} F(u, w) &= \overline{E}_{xp}/\overline{J} \\ &= -\sum_j \frac{1}{\rho_j^2}\left(\frac{uk_{zj}^2}{w} + \omega\mu_0 v_j Y_j\right)(\overline{E}_{jp}/\overline{J}) \end{aligned} \tag{12}$$

where $j = +$ or $-$, and where $(\overline{E}_{jp}/\overline{J})$ is defined as indicated in (11). Alternately, $F(u, w)$ can be defined as $\overline{E}_{xn}/\overline{J}$ which is numerically the same as (12) because of the continuity of $\overline{E}_x$ at $y = 0$.

Under conditions where $\epsilon_2 \to 0$, $F(u, w)$ of (12) simplifies to

$$F(u, w) = -\frac{1}{2(\epsilon_1 k_0^2 - w^2)}\left[\frac{u^2w^2}{\omega\epsilon_0\epsilon_1 v_+} + \omega\mu_0 v_-\right] \tag{13}$$

where v_+ and v_- are computed from (7).

III. Impedance Formulation

The driving point impedance of a flat strip antenna is computed from the expression

$$Z_v = -\frac{1}{[I(x = 0)]^2}\int_{-l}^{l}\int_{-\epsilon}^{\epsilon} E_x(x, z)J_x(x, z)dx dz. \tag{14}$$

TABLE I

IMPEDANCE DATA FOR $\Omega_c=\omega_c/\omega_p=1.5$

$\frac{\omega}{\omega_p}$	Trial Functions of Current	ϕ_t (degrees)	Z_v	$Z(l)$	$\left\|\frac{Z(l)}{Z_v}\right\|$	$0.1l\leq x_1\leq 0.95l$	
						$R(x_1)$	$X(x_1)$
1.4	3 terms (A_1, A_2, $A_3\neq 0$)	75	$302+i50.6$	$368+i62.1$	1.22	267 to 367	38 to 64
	2 sines ($A_2=0$)	75	$298+i65.6$	$389+i72$		252 to 360	56 to 81
	sine+cosine ($A_3=0$)	75	$259+i37.3$	$274+i12.6$		209 to 316	11 to 69
	3 terms (A_1, A_2, $A_3\neq 0$)	0	$295+i27.5$	$401+i12.9$	1.34		
1.475	3 terms (A_1, A_2, $A_3\neq 0$)	75	$6.6+i24.4$	$6.6+i43.9$	1.75	5.7 to 7.9	15.5 to 35
	2 sines ($A_2=0$)	75	$6.6+i24.2$	$6.7+i43.9$		5.6 to 7.9	15.4 to 35
	sine+cosine ($A_3=0$)	75	$37.8-i30.8$	$51.8-i38$		12 to 50	-45 to 17
	3 terms (A_1, A_2, $A_3\neq 0$)	0	$7.3+i23.9$	$7.3+i48$	1.94		

The electric field E is related to the surface current density of the antenna J by a tensor Green's function which is nonsymmetrical if a contribution to the field component E_i by the current density J_j differs from the contribution to E_j by J_i. However, there is no need to further investigate the structure of the dyadic functions if the net current of the flat strip antenna is represented by a single vector component. In this limit it can be shown that (14) is stationary with respect to small changes of the surface current density J_x or of the current $I(x)=\int_{-\epsilon}^{\epsilon}J_x(x, z)dz$ about its correct value [10]. The stationary character of the impedance (14) can be verified also by examining the Z_v data of Table I which exhibit smaller changes than the nonstationary $Z(l)$ values.

It is implied that only the component $J_x(x, z)$ is impressed by the source. The H_x field components were assumed to be continuous across the antenna surface at $y=0$ in the derivation of (11) and (12). This boundary condition requires that the transverse surface current densities on the two sides of a metallic antenna are related as $J_z(x, 0^+, z)=-J_z(x, 0^-, z)$. The analysis allows for a current that circulates around the transverse dimension of the strip, and it is possible to compute this current density by inverting the transform $\overline{H}_{xj}$ of (3). However, there is no need to account for these equal and opposite currents (which do not add to the net current flow) in the trial functions of the antenna current.

The surface current density is assumed to be an even function about $x=0$, $z=0$. Application of (1), (10), and (12) results in

$$Z_v = -\frac{1}{[2\pi I(x=0)]^2}\int_{-\infty}^{\infty}\int_{-\infty}^{\infty} du\,dw\,F(u, w) \left[\int_{-l}^{l}\int_{-\epsilon}^{\epsilon} J_x \cos ux \cos wz\,dx\,dz\right]^2. \quad (15)$$

The surface current density $J_x(x, z)$ is approximated by modified sine and shifted cosine functions

$$J_x(x, z) = f(z)\sum_{j=1}^{3} A_j f_j(x) \quad (16)$$

with

$$f(z) = 1/(2\epsilon), \qquad f_2(x) = 1 - \cos k_2(l - |x|)$$

and

$$f_j(x) = \begin{cases} \sin k_j(l - |x|) & \text{for } |x| \leq x_t \\ q_j\sqrt{l - |x|}\,[1 + a_j(l - |x|) + b_j(l - |x|)^2] & \text{for } |x| > x_t \end{cases} \quad (17)$$

where $j=1$ or 3. The parameters q_j, a_j, and b_j are determined by requiring that $f_j(x)$ and its first and second derivatives are continuous at $x=x_t$. Such a modification of the sine functions makes the resulting current proportional to the square root from the distance to the nearby antenna end, which is in line with the free space edge conditions of diffraction theory [11]. For antennas in free space, this modification avoids the strong tangential electric fields that are observed with a linearly decaying current near the antenna ends [7]. The degree of current nonlinearity can be controlled by changing the parameter x_t; $f_j(x)$ of (17) simplifies to an unmodified sine function for $x_t=l$. For the antenna orientation investigated in this paper, the modification of the sine function ($x_t\neq l$) is shown to be of little consequence in Section IV-D. However, this modification is of more significance for antennas oriented with their axis and surface parallel to the direction of the static magnetic field [12]. It is not claimed that a current distribution of form (17) satisfies edge conditions for an anisotropic medium; this paper merely investigates the effects of x_t variations on the antenna surface fields and impedance. Substituting (16) in (15), the impedance Z_v becomes

$$Z_v = \frac{\sum_{i=1}^{3}\sum_{j=1}^{3} A_i A_j \gamma_{ij}}{\left(\sum_{j=1}^{3} A_j F_j\right)^2} = \frac{N}{D^2} \quad (18)$$

where

$$\gamma_{ij} = -\frac{1}{\pi^2}\int_{-\infty}^{\infty}\int_{-\infty}^{\infty} du\,dw F(u, w) g_i(u) g_j(u \left(\frac{\sin \epsilon w}{\epsilon w}\right)^2 \quad (19)$$

$$g_j(u) = \int_0^l f_j(x)\cos ux\,dx \quad (20)$$

$$F_j = f_j(0). \quad (21)$$

The integrals (20) can be evaluated, and $g_2(u)$ involves sine functions, while $g_1(u)$ and $g_3(u)$ involve trigonometric functions and Fresnel integrals. The double integrals γ_{ij} remain to be evaluated numerically.

The impedance (18) is a function of the trial function amplitudes A_j. Because of the stationary character of (14), the optimum values of A_j are determined from the condition $dZ_v/dA_j=0$. This leads to

$$\frac{\sum_{j=1}^{3} A_j\gamma_{ij}}{F_i} = \frac{N}{D} \tag{22}$$

which remains constant for any value of i. Equation (22) represents three linear algebraic equations ($i=1$, 2, and 3), which can be combined into two linear nonhomogeneous equations for computing the complex amplitude ratios (A_2/A_1) and (A_3/A_1). Consequently, (18) gives an impedance figure Z_v for each assumed set of trial functions $f_1(x)$, $f_2(x)$, and $f_3(x)$.

The integrated electric fields are determined from an x-dependent impedance figure

$$Z(x_1) = -\frac{1}{2\epsilon I(0)}\int_{-\epsilon}^{\epsilon} dz \int_{-x_1}^{x_1} E_x(x)dx \tag{23}$$

where $x_1<l$. Substituting (1) and (12) in (23) and making use of (10) and (16) it follows that

$$Z(x_1) = \frac{\sum_{j=1}^{3} A_jV_j(x_1)}{\sum_{j=1}^{3} A_jF_j} \tag{24}$$

where

$$V_j(x_1) = -\frac{1}{\pi^2}\int_{-\infty}^{\infty}\int_{-\infty}^{\infty} du\, dw F(u,w)g_j(u) \cdot \frac{\sin ux_1}{u}\left(\frac{\sin \epsilon w}{\epsilon w}\right)^2. \tag{25}$$

The trial function amplitudes A_j have been determined from a solution of (22). $V_j(x_1)$ of (25) is functionally similar to γ_{ij} of (19). The computational routines used for calculating the integrals of γ_{ij} can be directly applied to the evaluation of $V_j(x_1)$. $Z(x_1)$ of (24) can be computed as readily as Z_v of (18).

IV. Discussion of Numerical Results

A. Uniaxial Medium

The magnetionic plasma degenerates into a uniaxial medium with $\epsilon_1=1$ and $\epsilon_2=0$ in the presence of strong magnetic fields ($\omega_c/\omega_p\to\infty$). For such a medium the antenna impedance is shown in Fig. 1, where the antenna and plasma parameters are similar to the ones used in the calculations leading to Fig. 2 of [2]. However, the present calculations are based on the antenna trial functions (16), where $\phi_i=k_j(l-x_i)$ designates the electric distance from the antenna tip where the sine terms of (17) are changed into a sum of odd powers of $\sqrt{l-|x|}$. The thin-line curves are computed with the modified sine current distribution of (17) by setting $A_2=A_3=0$ in (18). The broad lines refer to the closed form approximations derived in the Appendix for an assumed triangular current distribution. A comparison with Fig. 2 of [2] indicates lower resistance values near $\omega=\omega_p$ for the present computations. For $\omega\to\omega_p$, $|\epsilon_3|$ is decreased in magnitude, the lower limit of the w-integral of (29) approaches the upper limit, which results in numerically small values of R_+ near $\omega=\omega_p$. (The subsequent approximation (30) is not valid for $|\epsilon_3|\to 0$.) For an antenna oriented with the surface perpendicular to the static magnetic field, the resistance expressions (44) and (45) of [2] are inversely proportional to $\sqrt{|\epsilon_3|}$; and the antenna resistance should become large as $\omega\to\omega_p$. The closed-form approximations of the resistance are in agreement with numerical results by Seshadri [3] in the limit of $\omega\ll\omega_p$ who also noted small values of the effective antenna resistance at $\omega=\omega_p$.

Large resistance values are noted for $\omega<\omega_p$, which corresponds to the frequency range of gyromagnetic resonances, where a point dipole of arbitrary orientation would exhibit an infinite input resistance in a lossless plasma [13]. These large resistance values have been attributed in the quasi-static calculations of Balmain [4] to extended near fields of the antenna. For a lossy plasma, these extended near fields characterize power dissipation in the vicinity of the antenna, but the distant power flow remains similar to the one observed at higher frequencies. For an antenna oriented in a direction parallel to the static magnetic field, a similar behavior of the effective power flow has been noted by the author [14].

The inductive reactance of [2] corresponds to a capacitive reactance for $\omega<\omega_p$ in Fig. 1. A capacitive reactance has been noted by Balmain [4] for a cylindrical current element.

The different impedance characteristics for antennas oriented with their surfaces parallel and perpendicular to the static magnetic field can be explained qualitatively by examining the dielectric tensor near the antenna surface. For a strip antenna, the tangential electric surface fields should be equal to zero and the normal field components will predominate in the vicinity of the antenna surface. For antennas perpendicular to the static magnetic field [2], the z-component is perpendicular to the antenna surface and the electric displacement component ϵ_3E_z will be dominant near the antenna surface. For antennas parallel to the static magnetic field, the y-component is perpendicular to the antenna surface and the electric displacement component ϵ_1E_y is dominant. In a uniaxial medium $\epsilon_1=1$ and ϵ_3 has a large negative real part for low frequencies; for the static magnetic field parallel to the antenna surface, the antenna reactance should be closer to the free space conditions than for the antenna oriented with its surface perpendicular to the magnetic field. A capacitive reactance has been observed for the parallel antenna orientation but the reactance is of opposite sign for the perpendicular antenna orientation in [2]. However, for high frequencies, ϵ_3 approaches 1 and the antenna impedances should be comparable in both configurations.

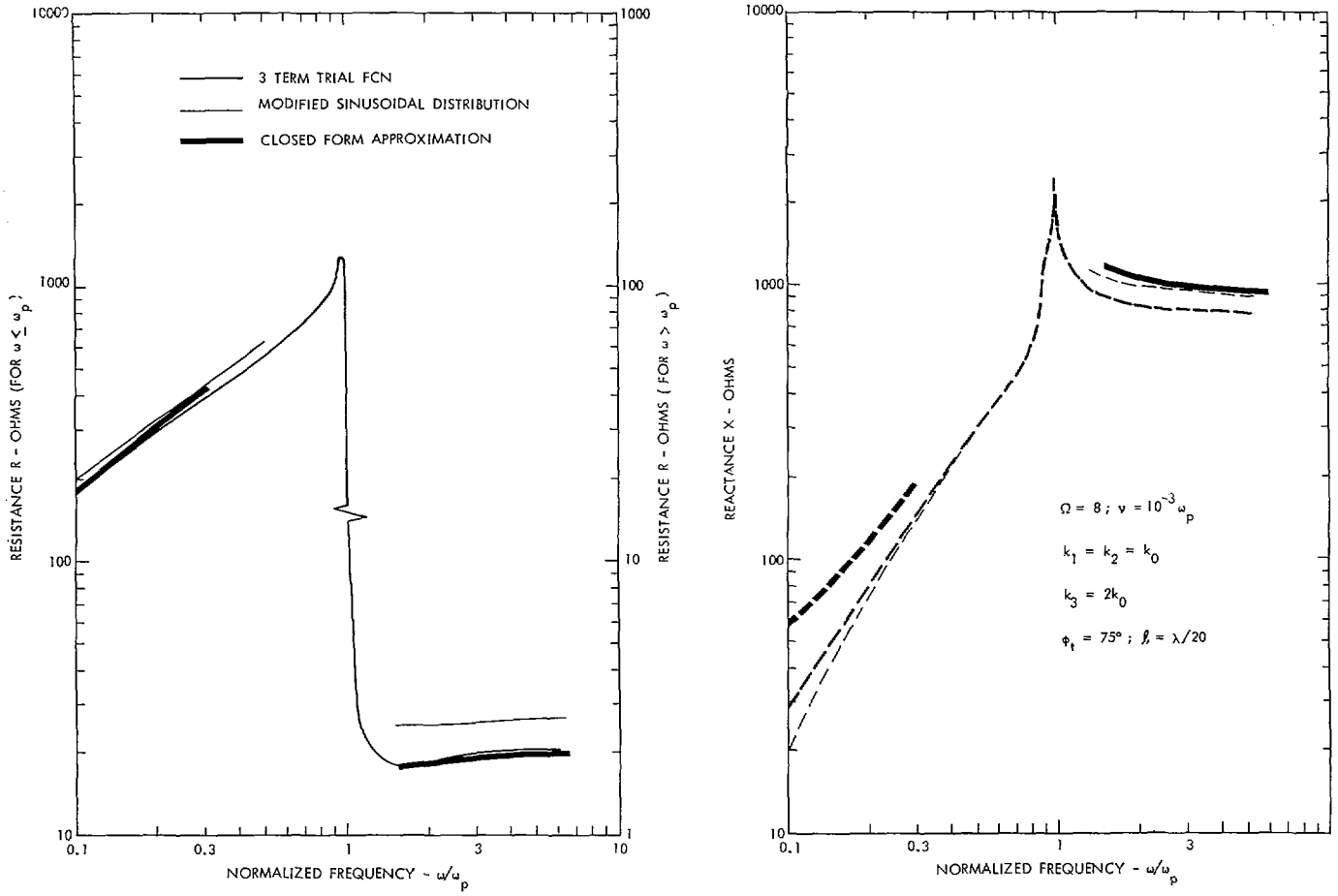

Fig. 1. Impedance of a short antenna in a uniaxial medium.

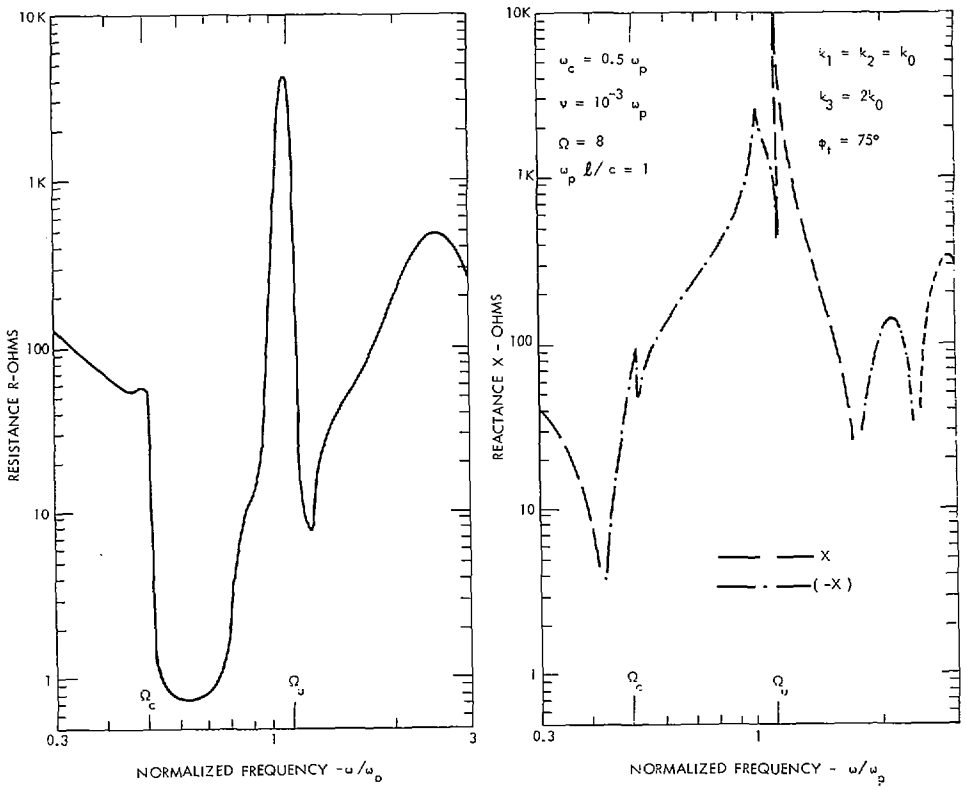

Fig. 2. Antenna impedance for $\Omega_c = \omega_c/\omega_p = 0.5$.

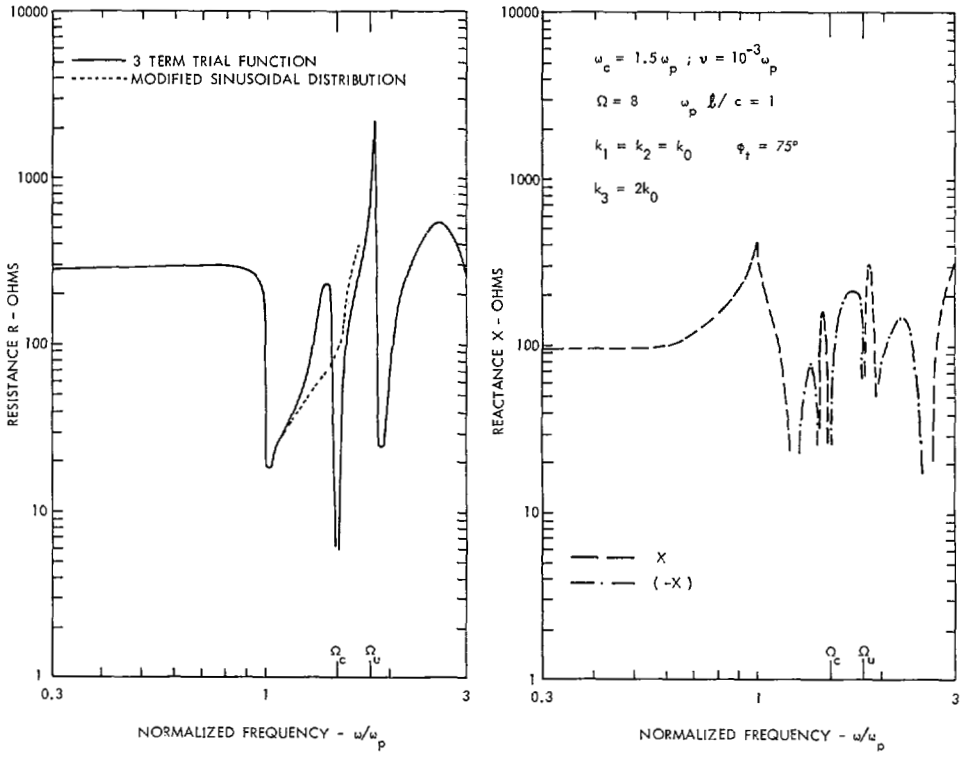

Fig. 3. Antenna impedance for $\Omega_c=\omega_c/\omega_p=1.5$.

B. Antenna Impedance for a Finite Magnetic Field

The driving point impedances are computed for an antenna length $l=c/\omega_p(l=\lambda/2\pi$ at $\omega=\omega_p)$, and the antenna parameters of Figs. 2 and 3 are the same as in Figs. 4 and 5 of [2].

For $\omega_c/\omega_p=0.5$ the impedance shown in Fig. 2 is quite similar to the impedance of Fig. 4 of [2], except that the impedance of the present calculations is higher at the upper hybrid resonance $\omega_u=\sqrt{\omega_c^2+\omega_p^2}$, which is indicated as $\Omega_u=\omega_u/\omega_p$ in Fig. 2, than at the plasma frequency in ω_p. Also, the resistance exhibits large values for $\omega<\omega_c$ and for $\omega_p<\omega<\omega_u$ in Fig. 4 of [1] for the antenna oriented with its axis and surface parallel to the applied static magnetic field. These regions of high resistance remain similar for the different antenna orientations ([1], [2], and the present study) and can be attributed to gyromagnetic and plasma resonances of the medium [15], [16], and [13]. For $\omega_c<\omega_p$, there are directions for which the plane-wave components excited by the antenna exhibit an infinite propagation coefficient in the frequency ranges $\omega<\omega_c$ and $\omega_p<\omega_c<\omega_u$. These frequency ranges are associated with infinite input resistance to point dipoles. The range of low resistance shown in Fig. 2 corresponds to frequencies $\omega_c<\omega<\omega_1=0.5(-\omega_c+\sqrt{\omega_p^2+4\omega_c^2})$, where the antenna resistance is equal to zero for a lossless medium (Fig. 2 of [1]). The low-frequency reactance is capacitive in Fig. 2, but it was inductive in Fig. 4 in [2].

For $\omega_c/\omega_p=1.5$, high resistances are noted in the frequency range $\omega<\omega_p$ and $\omega_c<\omega<\omega_u$ in Fig. 3 which are the same as the ranges of high resistance seen in Fig. 4 of [1] or Fig. 5 of [2]. For $\omega_c>\omega_p$, these are the frequency ranges of gyromagnetic and plasma resonance. The resistance decreases for ω approaching ω_p in Fig. 3, while it exhibited a large peak in Fig. 5 of [2]. This difference is similar to the one noted for uniaxial media and was discussed in Section IV,*A*. For higher frequencies, the resistances are similar, except for a higher resistance peak at $\omega\approx\omega_u$ in Fig. 3. A sinusoidal current distribution ($A_2=A_3=0$ in (16), indicated by the dotted lines in Fig. 3) does not reproduce the resistance changes observed near the gyrofrequency ω_c, which is denoted as $\Omega_c=\omega_c/\omega_p$ in Fig. 3. This change of the resistance is similar to the one shown in Fig. 5 of [2], where it was attributed to the increase in the electrical antenna length (or resonances) as ω approached ω_c for $\omega>\omega_p$. The antenna reactance is capacitive for $\omega<\omega_p$ in Fig. 3.

The antenna impedance computed for the static magnetic field in the direction parallel to the antenna surface in Figs. 2 and 3 are similar to the impedances for the static magnetic field perpendicular to the antenna surface in Figs. 4 and 5 of [2], except that the low-frequency reactance is capacitive in the present study. The very-high-resistance peaks observed at $\omega=\omega_p$ in [2] are also absent in Figs. 2 and 3.

C. Current Distributions

For the antenna surfaces oriented in a direction perpendicular to the static magnetic field, resonances have been observed for ω approaching ω_c only if $\omega>\omega_p$, which is also evident from the current distributions shown in Figs. 6 and 7 in [2]. These current distributions of [2] compare qualitatively with a sine wave of a wave number $k_s=\sqrt{\sqrt{\epsilon_1}\sqrt{\epsilon_3}}k_0$. For the antenna surface oriented in the direction parallel to the

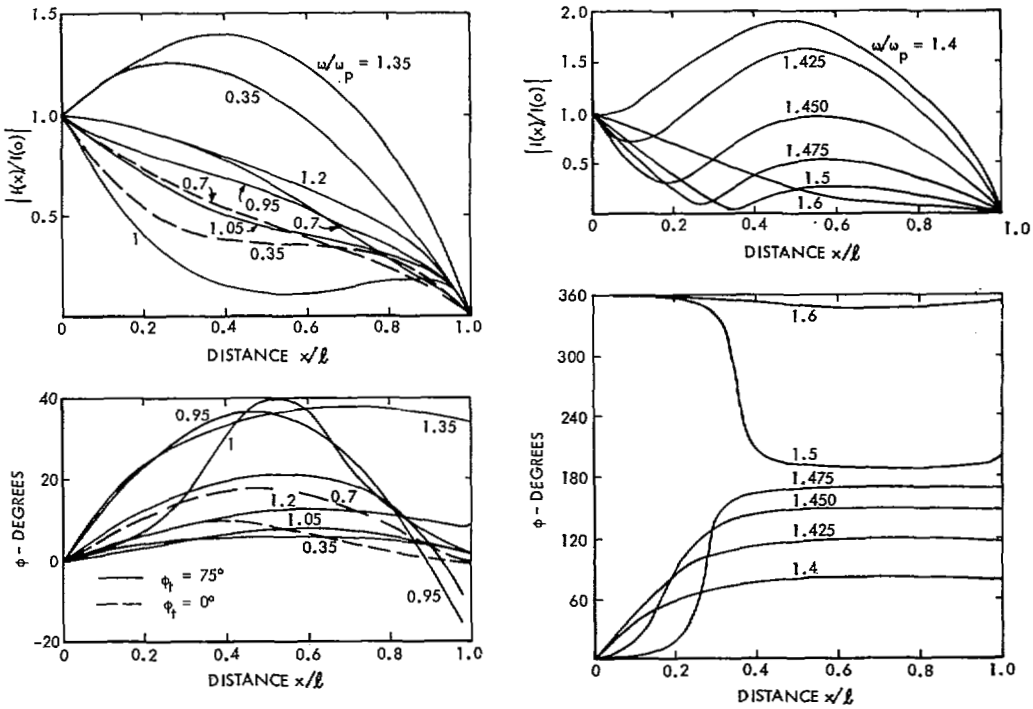

Fig. 4. Current distributions $|(x)=|(0)\exp(i\phi)$ for $\Omega_c=\omega_c/\omega_p=1.5$.

applied static magnetic field, approximate current distributions have been computed from (16), using the parameters shown in Figs. 2 and 3.

For $\omega_c=0.5\omega_p$ and $l=c/\omega_p$, the antenna current distribution is roughly the same as for a half-wave antenna in free space; for $0.45\omega_p<\omega<0.51\omega_p$, the current distribution approaches the triangular shape as ω is increased to $0.6\omega_p$. These current distributions are distinctly different from the current distributions in Fig. 6 of [2], which are attenuated along the antenna in the same frequency range.

For $\omega_c=1.5\omega_p$, a number of current distributions are indicated in Fig. 4. For $\omega\ll\omega_p$, the antenna current distributions exhibit only small phase angles, but their magnitude depends on the choice of $\phi_t=k_f(l-x_t)$; for $\omega/\omega_p=0.35$, $\phi_t=0$ gives an attenuated current distribution, but $\phi_t=75°$ produces an oscillatory curve. The impedances of the two sets of calculations, $Z_v=244+i\,99$ and $Z_v=283+i\,98$ ohms, differ less significantly because of the stationary impedance character. Still, the selected forms of the antenna current distributions do not appear satisfactory in the low-frequency limit. For higher frequencies ($\omega/\omega_p=0.7$), the differences between the current distributions computed for $\phi_t=0$ and 75° are smaller, and the corresponding impedances $Z_v=277+i139$ and $Z_v=288+i127$ differ less. The current distributions become nearly triangular in shape with increasing ω, and the current is attenuated along the antenna for $\omega=\omega_p$. The electrical antenna length is increased for $\omega>\omega_p$, and the phase variation of the current is also increased. For $\omega/\omega_p=1.4$, the current distribution indicates a larger electrical antenna length than the corresponding distribution of Fig. 7 of [2]. For $\omega/\omega_p=1.425$ and 1.45, the antenna current distributions approximate the magnitude and phase of current distributions of free space antennas of $l=\lambda/2$ and $5\lambda/8$ respectively. The current distribution decays in amplitude towards the end of the antenna for $\omega=1.475\omega_p$ in Fig. 4, while the current exhibits an oscillatory behavior in Fig. 7 of [2]. For $\omega/\omega_p=1.5$ and 1.6, the current distributions are similar to the ones shown for the same frequencies in Fig. 7 of [2].

There are frequency ranges where the antenna oriented with its surface parallel to the static magnetic field exhibits larger electrical length than the antenna oriented with the surface perpendicular to the static magnetic field. The wave number estimate k_s cannot be applied to the antenna current distributions considered in this paper, and alternate estimates have not been obtained.

D. Surface Fields

The x-dependent impedance $Z(x_1)$ of (23), which is proportional to the integral of the tangential electric fields $E_z(x)$ from $-x_1$ to x_1, has been computed to illustrate the degree to which the fields excited by the current distributions (16) approximate the desired boundary conditions of vanishing tangential electric fields on the antenna surface.

The impedance $Z(x_1)$ is shown in Fig. 5 for the current distributions of Fig. 4 with $\omega/\omega_p=1.4$ and 1.475. Horizontal lines indicate the components of the variationally computed driving point impedance $Z_v=R_v+iX_v$. Ideally $Z(x_1)=R(x_1)+iX(x_1)$ should be constant in the range of x_1 corresponding to points on the antenna surface. For the two frequencies shown in Fig. 5 the deviations of $R(x_1)$ and $X(x_1)$ from their average values are percentagewise smaller for $\omega=1.4\omega_p$, but smaller in magnitude for $\omega=1.475\omega_p$. Comparative variations of $Z(x_1)$ for a free space antenna

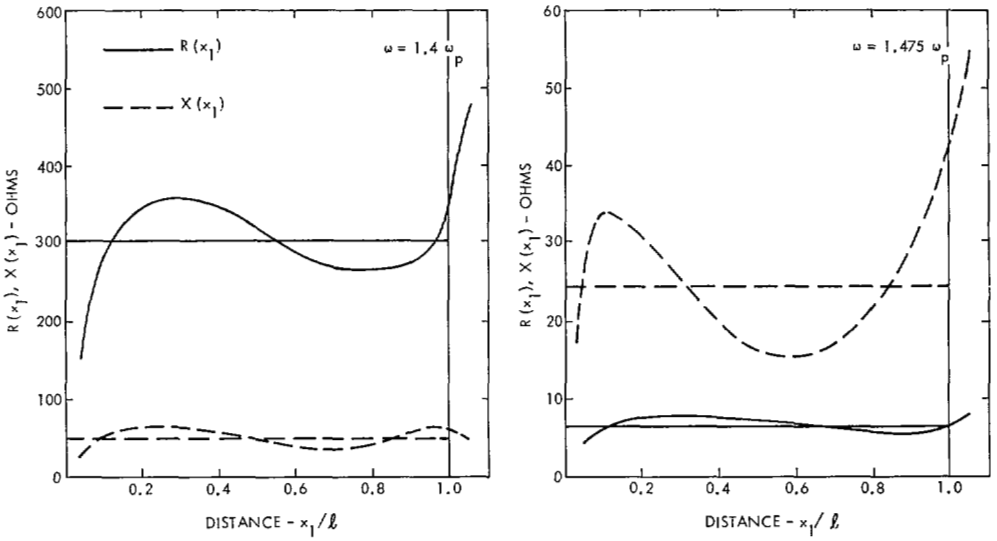

Fig. 5. Impedance $z(x_1)=R(x_1)+ix(x_1)$ for $\Omega_c=\omega_c/\omega_p=1.5$.

were shown to correspond to current distributions $I(x)$ and impedance figures Z_v that were verified experimentally [7].

The calculations reported in Fig. 5 have been made for a three-term current distribution (A_1, A_2, $A_3\neq 0$) with sine waves that are modified to exhibit $\sqrt{l-|x|}$ dependence near the antenna ends ($\phi_t=75°$). Table I compares these impedance data with calculations made using two term current distributions of two sine waves ($A_2=0$), sine waves and shifted cosine waves ($A_3=0$), and also with data for three-term current distributions having unmodified sine waves ($\phi_t=0°$).

For $\omega/\omega_p=1.4$, all the current distributions give comparable impedance data for $\phi_t=75°$. Also the fluctuations of $R(x_1)$ and $X(x_1)$ in the range of $0.1l\leq x_1\leq 0.9l$ are about the same in magnitude. The three-term current distribution using unmodified sine waves ($\phi_t=0°$) also provides a comparable impedance Z_v and $|Z(l)/Z_v|$ that is increased only slightly relative to $\phi_t=75°$.

For $\omega/\omega_p=1.475$, the impedances Z_v, $Z(l)$ and the fluctuations of $R(x_1)$ and $X(x_1)$ are comparable for the three-term functions and the two sine waves ($A_2=0$). The sine and shifted cosine wave gives an impedance $Z_v=R_v+iX_v$, where R_v is of different magnitude and X_v of different sign. Also the fluctuations of $R(x_1)$ and $X(x_1)$ are much larger for the sine and shifted cosine trial functions, and the Z_v impedance figures of the sine plus shifted cosine functions ($A_3=0$) can be discarded as unreliable. Obviously, the sine plus shifted cosine function with $k_1=k_2=k_0$ is not general enough to account for the oscillatory and decaying current function shown in Fig. 4 on a physically short antenna ($l=0.235\lambda$). Increasing the wave numbers to $k_1=k_2=2k_0$ gives $Z_v=8.1+i\,17.2$, which is in better agreement with the other results shown in Table I for $\omega/\omega_p=1.475$. The unmodified sine waves ($\phi_t=0°$) provide an impedance Z_v that is comparable to the impedance Z_v of the three-term trial functions with $\phi_t=75°$. The modification of the sine waves ($\phi_t\neq 0$), which was based on the free-space edge conditions, introduces a small change in the integrated surface fields or in the impedance $Z(l)$ for an antenna in a magnetoionic medium.

E. Summary of Conclusions

Antenna characteristics in a magnetoionic medium have been shown to depend on the antenna shape if the static magnetic field is applied in a direction perpendicular to the antenna axis. Earlier work [2] has examined a flat strip antenna with its surface perpendicular to the static magnetic field, while this paper considers a similar antenna with the static magnetic field in a direction parallel to its surface. The impedance characteristics of the antennas exhibit some differences in these two geometries, which have been correlated with differences in the electrically stored energy near the antenna surface. For the parallel direction of the static magnetic field and low frequencies, antenna reactance is capacitive, which is in an agreement with quasi-static calculations of Balmain [4] for a cylindrical current element. Also, there are no resistance peaks for frequencies ω near the plasma frequency ω_p, which was first observed by Seshadri [3] for a uniaxial medium.

Current distributions also differ for antennas oriented with their surfaces parallel and perpendicular to the applied static magnetic field—antennas are electrically longer for frequencies ω near the gyrofrequency ω_c, when the static magnetic field is parallel to the antenna surface.

The various antenna solutions have been checked by comparing the tangential electric surface fields with those originally postulated for the antenna excitation. The integral of the tangential electric fields along the antenna exhibits fluctuations, which are larger in magnitude for the less accurate current distributions. The integrated tangential fields fluctuate about a value corresponding to the antenna excitation voltage, which implies that the spatial average of the tangential electric fields is approximately equal to zero. This method of verifying antenna solutions appears novel and has not been used by any other authors.

Appendix

A Short Antenna in a Uniaxial Medium

For a sinusoidal current distribution, $A_2=A_3=0$ in (16) and $x_t=l$ in (17). The antenna impedance is expressed as

$$Z = -\frac{4}{(\pi \sin k_1 l)^2}\int_0^\infty \int_0^\infty F(u,w) g_1^2(u) \cdot\left(\frac{\sin \epsilon w}{\epsilon w}\right)^2 du\, dw \tag{26}$$

where $g_1(u)$ is defined by (50) of [1]. It can be separated in two parts $Z=Z_+ + Z_-$ corresponding with the two terms of $F(u, w)$ in (13), where the + and − subscripts refer to TM and TE modes, respectively. In the limit of k_1 approaching zero the current distribution along the antenna becomes triangular, and for ϵ_1 approaching 1 the real parts of the integral expressions Z_- and Z_+ can be seen to be identical to the radiation resistances (28) and (36) of Seshadri [3]. In the computation of $R_- = \mathrm{Re}\, Z_-$ the integrations are restricted to $u^2+w^2<k_0^2$. The integrals are evaluated after replacing the sine and cosine functions by their small argument approximations. It follows that

$$R_- = 15(k_0 l)^2. \tag{27}$$

In the computation of $R_+ = \mathrm{Re}\, Z_+$ for high frequencies ($\omega^2>\omega_p^2+\nu^2$), Re $\epsilon_3>0$ and the integrations are restricted to $u^2+\epsilon_3 w^2<\epsilon_3 k_0^2$. Applying the small argument approximations of the trigonometric functions,

$$R_+ = 5\epsilon_3 (k_0 l)^2. \tag{28}$$

The sum of (27) and (28) gives the same resistance as (50) of [2]. For low frequencies ($\omega^2<\omega_p^2+\nu^2$), Re $\epsilon_3<0$. Defining v^+ with Im $v^+>0$ it follows that

$$R_+ = \frac{2}{\omega\epsilon_0\epsilon_1\pi^2}\int_0^\infty \frac{du(\cos ul - 1)^2}{(ul)^2} \cdot \int_{u/\sqrt{|\epsilon_3|}}^\infty \left(\frac{\sin \epsilon w}{\epsilon w}\right)^2 \frac{dw}{\sqrt{|\epsilon_3| w^2 - u^2}}. \tag{29}$$

Assuming that $(\sin \epsilon w/\epsilon w)\approx 1$ near the lower limit of w it follows that

$$R_+ \approx \frac{2}{\omega\epsilon_0\epsilon_1\pi^2}\int_0^\infty \frac{du(\cos ul - 1)^2}{(ul)^2} \cdot\left[\frac{3}{2} - C - \log(\epsilon u) + \frac{1}{2}\log|\epsilon_3|\right] = \frac{120}{k_0 l\sqrt{|\epsilon_3|}} \cdot\left[\log\frac{2l}{\epsilon} + \frac{1}{2} - 2\log 2 + \frac{1}{2}\log|\epsilon_3|\right]. \tag{30}$$

For $\omega\ll\omega_p$ this closed-form approximation can be seen to give the same resistance values as the numerical calculations shown in Fig. 2(b) of Seshadri [3]. The resistance (30) differs by the last logarithmic term from the resistance (45) of [2] for an antenna where the static magnetic field is perpendicular to the antenna surface. For $\omega^2<(\omega_p^2+\nu^2)$, the reactance $X_+ = \mathrm{Im}\, Z_+$ is defined as

$$X_+ = \frac{2}{\omega\epsilon_0\epsilon_1\pi^2}\int_0^\infty du \frac{(\cos ul - 1)^2}{(ul)^2} \cdot \int_0^{u/\sqrt{|\epsilon_3|}} \left(\frac{\sin \epsilon w}{\epsilon w}\right)^2 \frac{dw}{\sqrt{u^2 - |\epsilon_3| w^2}}. \tag{31}$$

Over the range of integration shown in (31) the variable w is less than at the lower limit of (29), where it was permissible to replace $\sin \epsilon w/\epsilon w$ by 1. Applying the same approximation to (31), an elementary integration shows that

$$X_+ = \frac{60\pi}{k_0 l\sqrt{|\epsilon_3|}}. \tag{32}$$

This reactance is capacitive and is inversely proportional to the antenna length. The capacitive reactance of Balmain [4] is also inversely proportional to l, but for a cylindrical current element it is inversely proportional to $|\epsilon_3|$.

It is also possible to work out an approximate expression for $X_- = \mathrm{Im}\, Z_-$. This reactance of the TE modes is inductive and proportional to the antenna length. It becomes negligible relative to (32) in the limit of low frequencies.

References

[1] J. Galejs, "Impedance of a finite insulated cylindrical antenna in a cold plasma with a longitudinal magnetic field," *IEEE Trans. Antennas and Propagation*, vol. AP-14, pp. 727–736, November 1966.

[2] ——, "Impedance of a finite insulated antenna in a cold plasma with a perpendicular magnetic field," *IEEE Trans. Antennas and Propagation*, vol. AP-14, pp. 737–748, November 1966.

[3] S. R. Seshadri, "Radiation from a current strip in a uniaxially anisotropic plasma medium," *Can. J. Phys.*, vol. 44, pp. 207–217, January 1966.

[4] K. G. Balmain, "The impedance of a short dipole antenna in a magnetoplasma," *IEEE Trans. Antennas and Propagation*, vol. AP-12, pp. 605–617, September 1964.

[5] R. W. P. King, *Theory of Linear Antennas*. Cambridge, Mass.: Harvard University Press, 1956.

[6] R. F. Harrington, "Matrix methods for field problems," *Proc. IEEE*, vol. 55, pp. 136–149, 1967.

[7] J. Galejs, "Surface fields on linear antennas," *Proc. IEE* (London), vol. 115, pp. 627–632, May 1968.

[8] R. F. Harrington, *Time-Harmonic Electromagnetic Fields*. New York: McGraw-Hill, 1961, Section 7.9.

[9] E. Arbel, and L. B. Felsen, "Theory of radiation from sources in anisotropic media," in *Electromagnetic Waves*, Pt. 1, E. C. Jordan, Ed. New York: Pergamon, pp. 391–459, 1963.

[10] J. Galejs, *Antennas in Inhomogeneous Media*. New York: Pergamon, 1968.

[11] C. J. Bouwkamp, "Diffraction theory," *Rept. Prog. Phys.*, vol. 17, pp. 35–100, 1954.

[12] J. Galejs, "The insulated cylindrical antenna in a cold plasma with a longitudinal magnetic field," *IEEE Trans. Antennas and Propagation*, vol. AP-16, pp. 378–380, May 1968.

[13] S. R. Seshadri, "Radiation from an electric dipole in a magnetoplasma," *Can. J. Phys.*, vol. 44, pp. 3053–3067, 1966.

[14] J. Galejs, "Power flow from a short antenna in a lossy uniaxial medium," *Radio Science*, vol. 2, pp. 1419–1430, December 1967.

[15] S. R. Seshadri, "Wave propagation in a compressible ionosphere, I and II," *Radio Science*, vol. 68D, pp. 1285–1307, December 1964.

[16] ——, "Radiation resistance of elementary electric current sources in a magnetoionic medium," *Proc. IEE* (London), vol. 112, pp. 1856–1868, October 1965.